Hanle precession in the presence of energy-dependent coupling between localized states and an epitaxial graphene spin channel

van den Berg, J. J.; Kaverzin, A.; van Wees, B. J.

Published in:
Physical Review B

DOI:
10.1103/PhysRevB.94.235417

Publication date:
2016

Hanle precession in the presence of energy-dependent coupling between localized states and an epitaxial graphene spin channel

J. J. van den Berg,* A. Kaverzin, and B. J. van Wees
Physics of Nanodevices, Zernike Institute for Advanced Materials, University of Groningen, Nijenborgh 4, 9747 AG Groningen, The Netherlands
(Received 6 July 2016; revised manuscript received 9 November 2016; published 14 December 2016)

Hanle spin precession measurements are a common method to extract the spin transport properties of graphene. In epitaxial graphene on silicon carbide, these measurements show unexpected behavior, due to presumed localized states in the carbon buffer layer that is present between the channel and the substrate. As a consequence, the Hanle curve narrows in its magnetic field dependence and can show an unconventional shape, which has been experimentally observed and modeled in previous studies. Here, we extend the previously developed model by assuming that the localized states are charge traps, that have a power-law distribution of trapping times. Our simulations show that the energy dependence of these trapping times can be extracted from the temperature evolution of the Hanle curve, which was previously observed in experiments. Our extended model gives better insight into what processes play a role when a spin channel is coupled to localized states and their relation to the experimental observations.

DOI: 10.1103/PhysRevB.94.235417

I. INTRODUCTION

Epitaxial graphene on the silicon (0001) face of silicon carbide (SiC) [1–3] has been studied recently for its suitability as a spintronic material using Hanle spin precession experiments [4,5], which is a method to measure spin dynamics in a nonlocal spin valve geometry in the presence of an external, out-of-plane B field. It was observed that the spin transport properties are influenced by the presence of localized states in the buffer layer, an insulating carbon layer that is a characteristic feature of this material, resulting in a dramatic narrowing of the Hanle curve in the presence of the buffer layer [4,6]. More recently, even a change in the general shape of the Hanle curve was observed at low temperatures [7].

A previously developed model [6] explains both effects by assuming, coupled to the spin channel, localized states that briefly trap the itinerant spins. Simulations using the localized states model resemble the typical change in the Hanle curve that is seen in the experiments to some extent, but have some features that are different. So far, the localized states model succeeded in explaining the narrowing of the curve at high coupling strength (observed at room temperature) [6] and the development of an anomalous shape of the curve at intermediate coupling strength (observed at low temperatures) [7]. The exact shape of this anomalous Hanle curve, however, could not be properly simulated, indicating that the previously developed localized states model in the intermediate coupling regime is perhaps somewhat oversimplified. Also, a physical interpretation of the temperature dependence of the coupling rate has so far not been offered.

Here, we investigate further the shape of the Hanle curve within the scope of the previously developed model. To extend this model, we assume a coupling rate between the localized states and the channel that is not one specific value, but is distributed over a range of values, described by a distribution function $\mathcal{F}(\Gamma)$. We use for $\mathcal{F}(\Gamma)$ an inverse power-law distribution, derived from the heavy-tailed distribution of trapping times commonly found to describe dispersive transport [8,9]. We arrive at this distribution function by assuming an exponential dependence of the coupling rate on the energy E of the localized states away from the Fermi level. In this way, we can naturally explain the previously observed temperature dependence of the change in the shape of the Hanle curve.

With this analysis, we show that Hanle experiments are a means of obtaining insights about the nature of the localized states and the process that mediates the coupling with the channel. Furthermore, this generalized model can be used to describe any spin channel with localized or trapped states influencing the transport, and could therefore be of interest for the understanding of spintronics in organic semiconductors.

II. LOCALIZED STATES MODEL

We start with a brief summary of the previously developed model of localized states that are coupled to the spin channel [6], which we will later on refer to as the "reference model." The itinerant spins in the channel have a probability to hop into such a localized state and be trapped there for some trapping time t_t. While being immobilized, the spins can still relax and, in the presence of an applied magnetic field, precess. When there is a sufficiently large amount of these localized states, or groups of localized states, the spin dynamics in the system can be described using a spin accumulation in the channel, $\vec{\mu}_S$, and in the localized states, $\vec{\mu}_S^*$. The latter is a continuous variable if there are enough states available, a fact that can be justified if we consider that the buffer layer is a nonconducting but graphene-like layer.

Now, the situation can be expressed using two coupled Bloch equations, given by

$$\begin{aligned} 0 &= D\nabla^2\vec{\mu}_S - \frac{\vec{\mu}_S}{\tau_S} + \vec{\omega}_L \times \vec{\mu}_S - \eta\Gamma(\vec{\mu}_S - \vec{\mu}_S^*), \\ 0 &= -\frac{\vec{\mu}_S^*}{\tau_S^*} + \vec{\omega}_L^* \times \vec{\mu}_S^* - \Gamma(\vec{\mu}_S^* - \vec{\mu}_S). \end{aligned} \tag{1}$$

*j.j.van.den.berg@rug.nl

Here, D is the diffusion coefficient, τ_S the spin relaxation time, and ω_L the Larmor precession frequency. The $*$ denotes the properties of the localized states. The constant $\eta = \nu_{LS}/\nu$ is the ratio between the density of states (DOS) of the localized states and the DOS in the channel, and $\Gamma = 1/t_t$ is the coupling rate.

The effect of the localized states on $\vec{\mu}_S$ can be described by rewriting the two coupled Bloch equation into one, effective Bloch equation [6]:

$$0 = D\nabla^2\vec{\mu}_S - \frac{\vec{\mu}_S}{\tau_S^{\text{eff}}} + \vec{\omega}_L^{\text{eff}} \times \vec{\mu}_S, \tag{2}$$

with

$$\frac{1}{\tau_S^{\text{eff}}} = \frac{1}{\tau_S} + \eta\Gamma\frac{1+\tau_S^*\Gamma+(\tau_S^*\omega_L^*)^2}{(1+\tau_S^*\Gamma)^2+(\tau_S^*\omega_L^*)^2}, \tag{3}$$

$$\omega_L^{\text{eff}} = \omega_L + \eta\Gamma^2\frac{(\tau_S^*)^2\omega_L^*}{(1+\tau_S^*\Gamma)^2+(\tau_S^*\omega_L^*)^2}. \tag{4}$$

As described in Ref. [6], the expression of Eq. (3) and Eq. (4) can be simplified by considering different coupling regimes. This is done by comparing the coupling rate Γ with the other characteristic rates in the system, $1/\tau_S$ and ω_L. When these rates are much larger than Γ, spins that hop into the localized states will be lost due to relaxation or dephasing, respectively. However, the regime of strong coupling ($\Gamma \gg 1/\tau_S^*$) and low precession frequency ($\Gamma \gg \omega_L^*$) is typically the regime of interest for our system, at least at room temperature. In this regime, Eq. (3) and Eq. (4) can be simplified into $1/\tau_S^{\text{eff}} = 1/\tau_S + \eta/\tau_S^*$ and $\omega_L^{\text{eff}} = \omega_L + \eta\omega_L^*$. These effective parameters τ_S^{eff} and ω_L^{eff} result in a Hanle curve that is very narrow compared to the conventional case of a channel without localized states, but the curve maintains its shape.

In Ref. [7], the regime of intermediate coupling was considered, where $\eta\Gamma \sim 1/\tau_S$. In this regime, the complex interdependence of τ_S^{eff} and ω_L^{eff} results in a nontrivial change of the shape of the Hanle curve, which in that work was experimentally shown at low temperatures down to 4 K.

Extension of the model: Localized states with varying coupling rate

Now, we investigate what happens if Γ changes as a function of the position x in the channel. In this approach, which we will call the "extended model," the system can be described as a channel where the localized states have a changing coupling rate Γ_i depending on the specific location in the channel, as shown in Fig. 1. We make the assumption that the spin dynamics in the systems can be described in terms of the spin accumulation $\vec{\mu}_S$ and a spin accumulation $\vec{\mu}_{S,i}$, associated with all localized states or groups of localized states with coupling rate Γ_i. The quantity η_i describes the ratio between the DOS of the localized states with Γ_i and the DOS in the channel.

Because we consider a large number of localized states and a continuous variable $\vec{\mu}_S$, the system behaves as a channel which is coupled to different types of localized states that couple at the same location simultaneously, where we maintain the assumption that there is no hopping between the localized states. Now, we can extend the reference model by simply adding extra coupled Bloch equations describing the spin

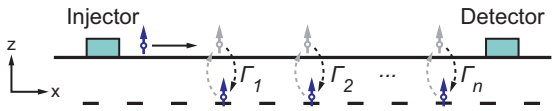

FIG. 1. Schematic representation of a diffusive spin channel where spins can be trapped in localized states coupled to the channel. In the model presented here, the coupling rate Γ can be different from trap to trap. We model this by n distinctive states, which each have a different coupling rate. The effective spin transport properties can then be calculated by a summation over the contributions of all localized states.

accumulation in the system. For n different types of localized states we are now left with $n+1$ coupled equations. In this notation we have replaced the spin accumulation in the localized states $\vec{\mu}_S^*$ that was used in the reference model with $\vec{\mu}_{S,i}$. For the corresponding properties we also replace the $*$ with the index i:

$$\begin{aligned}
0 &= D\nabla^2\vec{\mu}_S - \frac{\vec{\mu}_S}{\tau_S} + \vec{\omega}_L \times \vec{\mu}_S - \eta_1\Gamma_1(\vec{\mu}_S - \vec{\mu}_{S,1}) \\
&\quad - \eta_2\Gamma_2(\vec{\mu}_S - \vec{\mu}_{S,2}) - \cdots - \eta_n\Gamma_n(\vec{\mu}_S - \vec{\mu}_{S,n}), \\
0 &= -\frac{\vec{\mu}_{S,1}}{\tau_{S,1}} + \vec{\omega}_{L,1} \times \vec{\mu}_{S,1} - \Gamma_1(\vec{\mu}_{S,1} - \vec{\mu}_S), \\
0 &= -\frac{\vec{\mu}_{S,2}}{\tau_{S,2}} + \vec{\omega}_{L,2} \times \vec{\mu}_{S,2} - \Gamma_2(\vec{\mu}_{S,2} - \vec{\mu}_S), \\
&\cdots \\
0 &= -\frac{\vec{\mu}_{S,n}}{\tau_{S,n}} + \vec{\omega}_{L,n} \times \vec{\mu}_{S,n} - \Gamma_n(\vec{\mu}_{S,n} - \vec{\mu}_S).
\end{aligned} \tag{5}$$

We can rewrite $0 = -\vec{\mu}_{S,i}/\tau_{S,i} + \vec{\omega}_{L,i} \times \vec{\mu}_{S,i} - \Gamma_i(\vec{\mu}_{S,i} - \vec{\mu}_S)$ as $\vec{\mu}_{S,i} = a_i\vec{\mu}_S$, following the same method as for the reference model for one type of localized states [6]. Thus we can rewrite the first line of Eq. (5), which describes the spin accumulation in the channel, as

$$\begin{aligned}
0 = D\nabla^2\vec{\mu}_S - \frac{\vec{\mu}_S}{\tau_S^{\text{eff},1}} + \vec{\omega}_L^{\text{eff},1} \times \vec{\mu}_S - \eta_2\Gamma_2(\vec{\mu}_S - \vec{\mu}_{S,2}) \\
- \cdots - \eta_n\Gamma_n(\vec{\mu}_S - \vec{\mu}_{S,n}),
\end{aligned} \tag{6}$$

using the same procedure as for Eq. (2). Iterating this step n times yields an effective Bloch equation that takes into account the contributions of all types of localized stated. This gives

$$0 = D\nabla^2\vec{\mu}_S - \frac{\vec{\mu}_S}{\tau_S^{\text{eff},n}} + \vec{\omega}_L^{\text{eff},n} \times \vec{\mu}_S \tag{7}$$

with

$$\frac{1}{\tau_S^{\text{eff},n}} = \frac{1}{\tau_S} + \sum_{i=1}^{n}\eta_i f(\Gamma_i), \tag{8}$$

$$\omega_L^{\text{eff},n} = \omega_L + \sum_{i=1}^{n}\eta_i g(\Gamma_i), \tag{9}$$

using for convenience the following newly introduced functions:

$$f(x) \equiv x\frac{1+\tau_S^*x+(\tau_S^*\omega_L^*)^2}{(1+\tau_S^*x)^2+(\tau_S^*\omega_L^*)^2} \tag{10}$$

and

$$g(x) \equiv x^2 \frac{(\tau_S^*)^2 \omega_L^*}{(1+\tau_S^* x)^2 + (\tau_S^* \omega_L^*)^2}. \tag{11}$$

Not to complicate things further, we made here the assumption that the spin relaxation time in all the localized states is constant $\tau_{S,i} = \tau_S^*$. We also used $\omega_{L,i} = \omega_L^*$, because there is no reason to believe a significant variation in the g factor.

We can interpret η_i as the weighing factor of the different contributions, meaning that for each Γ_i there is a corresponding $\eta_i = \eta(\Gamma_i)$. In other words, the weighing factor is in fact a Γ-dependent variable $\eta(\Gamma)$. As a consequence, we have to change notation and now define the constant $\eta_0 = \nu_{LS}/\nu$ as the ratio between the DOS of all localized states and the DOS in the channel (where we previously used η), in order to keep the description consistent with the reference model. Hence, η_0 is now defined as the ratio between the localized states DOS and the DOS in the channel, summed over all types of localized states:

$$\sum_{i=1}^{n} \eta_i = \sum_{i=1}^{n} \eta(\Gamma_i) = \eta_0. \tag{12}$$

For a large n, we can consider Γ to be a continuously distributed parameter, described by some distribution function $\mathcal{F}(\Gamma)$. This distribution function is closely related to the weighing factor via the expression $\eta(\Gamma_i) = \mathcal{F}(\Gamma_i)\Delta\Gamma$. This allows us to rewrite the summation terms in Eq. (8) and Eq. (9) as an integral, by taking the limit $n \to \infty$, giving

$$\frac{1}{\tau_S^{\text{eff}}} = \frac{1}{\tau_S} + \int_\Gamma \mathcal{F}(\Gamma) f(\Gamma)\, d\Gamma, \tag{13}$$

$$\omega_L^{\text{eff}} = \omega_L + \int_\Gamma \mathcal{F}(\Gamma) g(\Gamma)\, d\Gamma. \tag{14}$$

The continuous version of Eq. (12) is given by

$$\lim_{n\to\infty} \sum_{i=1}^{n} \eta(\Gamma_i) = \int_\Gamma \mathcal{F}(\Gamma)\, d\Gamma = \eta_0. \tag{15}$$

Thus, using this description we can investigate any distribution function $\mathcal{F}(\Gamma)$ describing the spreading in the coupling rate Γ, while keeping the ratio η_0 constant. Note that the distribution function given by $\mathcal{F}_D(\Gamma) = \eta_0 \delta(\Gamma - \Gamma_0)$, where $\delta(\Gamma)$ is the Dirac delta function, returns the original results described in Eqs. (3) and (4), where we changed notation from Γ (which is now a variable) to Γ_0.

III. INVERSE POWER-LAW DISTRIBUTION FOR $\mathcal{F}(\Gamma)$

To find out what type of distribution function $\mathcal{F}(\Gamma)$ would correctly describe our system, we look in the literature for other systems with similar transport characteristics. A good candidate is offered by the well-studied disordered semiconductors that exhibit dispersive transport, characterized by free carriers that are immobilized in charge traps. These traps have a range of trapping times that are described by a power-law distribution [8,9]. The effect of this distribution of trapping times on spin transport in organic semiconductors was recently studied [10]. In this study the assumption was made

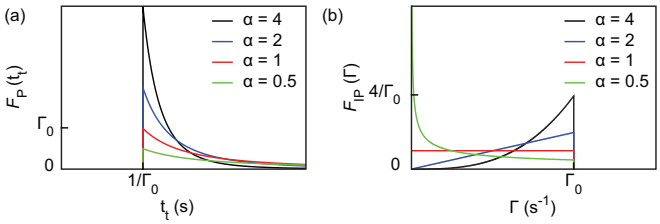

FIG. 2. (a) Power-law distribution for the trapping time $\mathcal{F}_P(t_t)$ for different tail indices α. (b) Inverse power-law distribution function for the coupling rate $\mathcal{F}_{IP}(\Gamma)$.

that electrons in traps do not undergo any spin relaxation, resulting in a strong narrowing and shape change of the Hanle curve.

The power-law distribution of trapping times is a direct consequence of charge traps that are exponentially distributed in energy E, where E is the activation energy that is required to leave the traps. Following Ref. [9], the dependence on energy of the DOS of the traps (to be more precise, its ratio with the DOS in the channel) $\eta(E)$ is then described by

$$\eta(E) = \eta_0 \exp\left(-\frac{E}{k_B T_C}\right), \tag{16}$$

with k_B Boltzmann's constant and T_C a characteristic temperature that gives the steepness of the energy distribution that describes the decline of the number of traps as the energy moves away from E_F. The coupling rate is given by

$$\Gamma(E) = \Gamma_0 \exp\left(-\frac{E}{k_B T}\right), \tag{17}$$

with T the temperature.

For the trapping time t_t, this results in a distribution $\mathcal{F}_P(t_t)$ that has a power-law decay [9], also known as the Pareto distribution. Because we consider $\Gamma = 1/t_t$, we deduce here the inverse of that distribution, $\mathcal{F}_{IP}(\Gamma)$ (see also Supplemental Material [11]):

$$\begin{aligned}\mathcal{F}_{IP}(\Gamma) &= \frac{d\eta}{dE}\frac{dE}{d\Gamma} \\ &= \eta_0 \alpha \Gamma_0^{-\alpha} \Gamma^{(\alpha-1)}, \quad \text{for } 0 \leqslant \Gamma \leqslant \Gamma_0.\end{aligned} \tag{18}$$

Here, we introduce the parameter $\alpha = T/T_C$, which is an index that gives the weight of the tail of $\mathcal{F}_P(t_t)$. Γ_0 can be physically related to the attempt-to-escape rate, which limits the maximum possible rate irrespective of the consideration of the particular energy barrier. It was estimated to be 10^{12} s^{-1} following Ref. [9]. In Fig. 2 we show both $\mathcal{F}_P(t_t)$ and $\mathcal{F}_{IP}(\Gamma)$ for different values for α. Thus, we have an energy-dependent distribution describing the coupling rate solely determined by the parameters T_C, η_0, and Γ_0, where the latter two replace the constant values for η and Γ that were used in the reference model.

IV. SIMULATIONS

Using the software MATLAB it is possible to simulate the effect of the distribution function in Eq. (18) on the Hanle curve. To obtain the full expressions for the effective properties

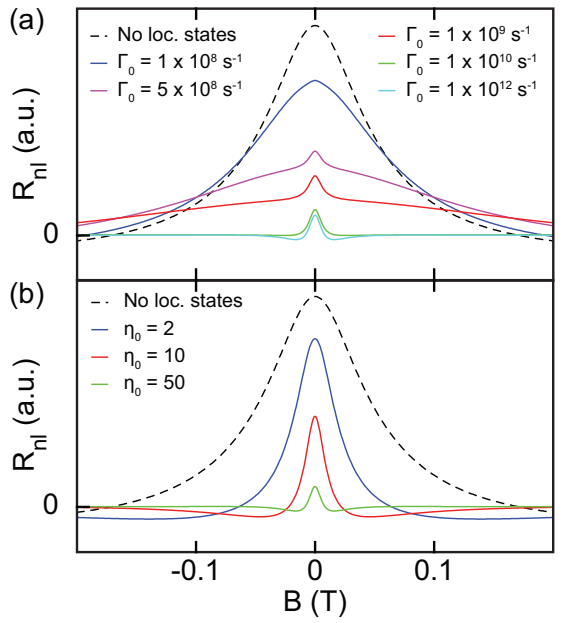

FIG. 3. (a) The effect on the Hanle curve of a different coupling rate Γ_0 in the extended model that includes the inverse power-law distribution function for the coupling rate. Used parameters for this plot: $D_C = 0.015\ m^2\ s^{-1}$, $\tau_S = 150$ ps, $L = 1\ \mu$m, $W = 1\ \mu$m, $\tau_S^* = 1$ ns, $\eta_0 = 50$, $T = 300$ K, $T_C = 200$ K. (b) The effect of a different ratio η_0 between the DOS of the localized states and the DOS in the spin channel. The used coupling rate $\Gamma_0 = 10^{12}\ s^{-1}$; other parameters used for this plot are the same as for (a).

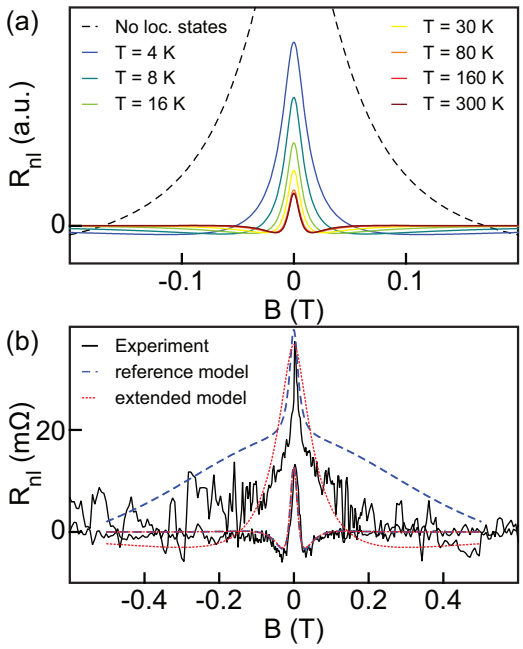

FIG. 4. (a) T-dependent simulations of the Hanle curve shape using the extended model. The tail index $\alpha = T/T_C$ puts more weight in the tail of the distribution function $\mathcal{F}(t_t)$, resulting in a bigger contribution of states with a low coupling rate. Thus at low T, many localized states fall in the intermediate coupling regime, changing the shape of the Hanle curve. T_C relates to the temperature above which the distribution function does not effect the shape. Used parameters in this plot: $D_C = 0.015\ m^2\ s^{-1}$, $\tau_S = 150$ ps, $L = 1\ \mu$m, $W = 1\ \mu$m, $\tau_S^* = 1$ ns, $\eta_0 = 50$, $\Gamma_0 = 10^{12}\ s^{-1}$, $T_C = 200$ K. (b) Comparison between the experiment (black solid lines, from Ref. [7]) and the two models: the reference model (blue dashed line, also Ref. [7]) and extended model (red dotted line) at different temperatures. For clarity, only the RT and 4 K curves are shown. The three narrow, overlapping curves are the RT measurements and simulations. The other three, wider curves are at low temperature. The used parameters in these simulations are for the reference model: $D_C = 0.02\ m^2\ s^{-1}$, $\tau_S = 150$ ps, $L = 1\ \mu$m, $W = 1\ \mu$m, $\tau_S^* = 0.42$ ns, $\eta_0 = 42$, $\Gamma_0 = 10^9\ /\ 10^{13}\ s^{-1}$. For the extended model, we used $D_C = 0.015\ m^2\ s^{-1}$, $\tau_S = 30$ ps, $L = 1\ \mu$m, $W = 1\ \mu$m, $\tau_S^* = 1$ ns, $\eta_0 = 31$, $\Gamma_0 = 10^{12}\ s^{-1}$, and $T_C = 200$ K.

τ_S^{eff} and ω_L^{eff}, we incorporate Eq. (18) into Eq. (13) and Eq. (14) and integrate over the whole range $0 \leqslant \Gamma \leqslant \Gamma_0$.

We show here the effect of changing the typical parameters T_C, η_0, and Γ_0. The rest of the parameters used in the model are based on the experimental results and analysis from previous studies.

Figure 3(a) shows how Γ_0 relates to the narrowing and/or shape change of the Hanle curve. For high coupling, there is a narrowing of the curve, while for intermediate coupling also the shape changes, as is consistent with the reference model. Also consistent with previous description, η_0 relates to the strength of the effect of narrowing and shape change of the Hanle curve in the limit at Γ_0. The effect is demonstrated in Fig. 3(b).

In Fig. 4(a) we show the role of T_C in the extended model. When increasing the temperature from the cryogenic region up to room temperature, the Hanle curve evolves from a shape that has some features of a conventional Hanle curve without the effect of localized states, into the final shape defined by Γ_0 and η_0. T_C relates to the typical temperature where the Hanle curves stops evolving and reaches the high coupling limit. Thus, for $T > T_C$, the Hanle curve can be described by the reference model in the high coupling limit. This can be intuitively seen in Fig. 2, where for large α the distribution functions become very selective and ultimately approach a delta function. Hence, the temperature evolution of the Hanle precession curve can show the steepness of the localized states decay with energy, by simply looking at the transition temperature between the intermediate and high coupling regime, or similarly, the transition between an anomalous shape and a narrowing of the curve.

In Fig. 4(b) we show a comparison between previously obtained experimental data (from Ref. [7]) and the two different models. The reference model (also from Ref. [7]) does not have an explicit dependence on T, but instead shows the curve for two different values of Γ. The extended model with the inverse power-law distribution $\mathcal{F}_{IP}(\Gamma)$, as described in this work, is shown for two different temperatures (RT and at 4 K). The measurements are shown by the black solid line. The three narrow Hanle curves show that both models have a good match at RT, as can be seen from their overlap with the experiment. The wider and larger curves are at cryogenic temperature. Here, the Hanle curve has an anomalous shape, and this is also where the models deviate from the experiment and from each other. The number of free parameters in both models, however, is too high for an unambiguous fit to the

data. The extension of the model allows for reproducing certain features of the measured curve, in a way that was not possible with the reference model. However, the model is limited in completely reproducing the experiment with a single set of parameters.

V. DISCUSSION AND CONCLUSIONS

To have an idea how strongly the extended model relies on the use of the proposed inverse power-law distribution, we also investigated the effect of other distribution functions $\mathcal{F}(\Gamma)$ on the spin transport properties and the Hanle curve. We found that using a constant spreading or a normal distribution did not have a significant effect on the Hanle curve shape, compared to the reference model. Likewise, a slightly skewed distribution such as the log-normal distribution did not effect the shape significantly either. The only type of distribution functions having a significant effect on the Hanle shape were functions with a large contribution from states in the regime of intermediate coupling, but with a significant weight of Γ spreading out over several orders of magnitude. Thus, power-law or inverse power-law distributions are suitable candidates to imitate the effect seen in experiment.

The fact that the extended model still deviates from the experimental data in Fig. 4(b) can have a number of reasons. A first reason could be that both energy-dependent functions $\eta(E)$, $\Gamma(E)$ are not purely exponential, but should be approximated by some other function, increasing the complexity of the distribution function $\mathcal{F}(\Gamma)$ and its temperature dependence. Second, the fact that we assume a constant (i.e., energy and temperature independent) relaxation time in the localized states τ_S^* might be an oversimplification of the physical situation. Third, there could be a significant spatial variation in the DOS of the localized states, as well as in their properties, depending on the physical origin of the localized states (e.g., strain, defects, dangling bonds, or a combination). Lastly, we did not incorporate the effect of tunneling between the localized states and the channel, which could play a role additional to the thermal hopping.

Even though a number of features could be added to extend the model further, it is important to note that already in our simplified description the number of degrees of freedom is too high to unambiguously determine all parameters with the available experimental data. To further understand the physical mechanisms that play a role, new experiments should be designed. More information about the most important variables could be obtained by employing different techniques, for example optical spin injection in a time-of-flight setup, electron spin resonance, or noise measurements.

To conclude, we introduced here an explanation for the temperature evolution of the Hanle curve in epitaxial graphene spin devices on SiC, by assuming hopping between the spin channel and charge traps. For this, we assume that the number of traps and their coupling rate exponentially decay with their energy difference with the Fermi level. The strength of this decay, defined by T_C, can be extracted from experiments by identifying the transition between narrowing of the Hanle curve at room temperature to an anomalous shape at lower temperatures. Our extended model thereby describes the temperature evolution of the Hanle line shape in a natural way. Comparing our simulations with previously measured experimental result showed that neither the reference localized states model nor the extended model can fully fit the measured curve, but both can capture certain features of the shape. Complementary experimental investigations are necessary to study in more detail the seemingly complex relationship between the anomalous Hanle line shape and the energy distribution of the localized states in an epitaxial graphene spin channel.

ACKNOWLEDGMENTS

We would like to acknowledge H. M. de Roosz, H. Adema, and J. G. Holstein for technical support. The research leading to these results has received funding from NanoNed, the Zernike Institute for Advanced Materials, and the European Union Seventh Framework Programmes under Grant Agreement "ConceptGraphene" (No. 257829) and "Graphene Flagship" (No. 604391).

[1] W. A. de Heer, C. Berger, X. Wu *et al.*, Epitaxial graphene, Solid State Commun. **143**, 92 (2007).

[2] K. V. Emtsev, F. Speck, T. Seyller, L. Ley, and J. D. Riley, Interaction, growth, and ordering of epitaxial graphene on SiC{0001} surfaces: A comparative photoelectron spectroscopy study, Phys. Rev. B **77**, 155303 (2008).

[3] U. Starke and C. Riedl, Epitaxial graphene on SiC(0001) and SiC(000-1): From surface reconstructions to carbon electronics, J. Phys.: Condens. Matter **21**, 134016 (2009).

[4] T. Maassen, J. J. van den Berg, N. IJbema *et al.*, Long spin relaxation times in wafer scale epitaxial graphene on SiC(0001), Nano Lett. **12**, 1498 (2012).

[5] B. Birkner, D. Pachniowski, A. Sandner, M. Ostler, T. Seyller, J. Fabian, M. Ciorga, D. Weiss, and J. Eroms, Annealing-induced magnetic moments detected by spin precession measurements in epitaxial graphene on SiC, Phys. Rev. B **87**, 081405(R) (2013).

[6] T. Maassen, J. J. van den Berg, E. H. Huisman, H. Dijkstra, F. Fromm, T. Seyller, and B. J. van Wees, Localized States Influence Spin Transport in Epitaxial Graphene, Phys. Rev. Lett. **110**, 067209 (2013).

[7] J. J. van den Berg, W. Strupinski, and B. J. van Wees, Observation of anomalous Hanle spin precession line shapes resulting from interaction with localized states, Phys. Rev. B **91**, 081403 (2015).

[8] H. Scher and E. W. Montroll, Anomalous transit-time dispersion in amorphous solids, Phys. Rev. B **12**, 2455 (1975).

[9] T. Tiedje and A. Rose, A physical interpretation of dispersive transport in disordered semiconductors, Solid State Commun. **37**, 49 (1981).

[10] R. C. Roundy and M. E. Raikh, Spin transport with dispersive traps: Narrowing of the Hanle curve, Phys. Rev. B **90**, 241202 (2014).

[11] See Supplemental Material at http://link.aps.org/supplemental/10.1103/PhysRevB.94.235417 for a derivation of $\mathcal{F}_{IP}(\Gamma)$.